Mechanisms of Flow Induced Vibrations of Circular Cylinders in Crossflow

S.V. Guerreiro Ribeiro
Center for Advanced Studies

J.E. Meyer
Department of Nuclear Engineering
Massachusetts Institute of Technology, Cambridge, Massachusetts 02139, U.S.A.

ABSTRACT

Two mechanisms of flow-induced vibration of circular cylinders are proposed. The first is based on the sharp decrease in the crossflow drag coefficient at Reynolds numbers of approximately $3x10^5$. The second is produced by the existence of a velocity gradient in the flow that crosses the cylinder. Stability criteria are developed by linearization of the nonlinear equations of motion for both mechanisms for several simple geometries. A computer code to solve the nonlinear equations of motion was developed and used to verify the stability criteria. The computer code was also applied to comparisons with experimental results representing both mechanisms. Good agreement with these experiments were obtained.

An actual case of steam-generator tube vibration which occurred in Ringhals 3, Sweden, is discussed. A possible explanation for the fretting scars on the tubes produced by the baffle plates is given based on one of the proposed mechanisms. A suggestion is made to correct the problem by increasing the surface roughness of the tubes. This roughening shifts the critical Reynolds number to a lower value intended to be outside the operating range for the steam generator.

1. Introduction

Unexpected steam generator tube vibrations were found in the nuclear power plants Ringhals 3 [1] and Almaraz [2] in Sweden and Spain, respectively. Since their design is similar to the Brazilian nuclear power plant, Angra 1, which is still in the mid-range power testing phase, the same problem is anticipated to occur at higher power levels. Apparently, the well-known fluid-induced vibration mechanisms, fluid elastic excitation, vortex shedding, and turbulence, are not responsible for the phenomenon [3].

Thus, we are motivated to investigate other possible mechanisms that may have caused the steam generator tube vibration. Since the flow conditions in the instability region are near the critical Reynolds number [1], we will propose a mechanism of flow-induced vibration of circular cylinders based on the sharp decrease in the drag coefficient past the critical Reynolds number [4], [5]. Experimental evidence is found in literature, some by accident as in the experiment performed by Humphreys [5]. He detected a structure resonance for Re near the critical range and above. Also, Lubin et al. [6], [7] observed in a tube bank vibration experiment that in the critical Re region an increase in the flow would decrease the vibration amplitude contrary to what has been previously observed. They mention a not clearly identified mechanism that produced periodic response. Also, as pointed out by Tietjens [8], page 98, "the sudden drop in the drag coefficient in the region of Reynolds number between 2×10^5 and 5×10^5 is so large that the drag itself, instead of increasing quadratically with the velocity, even decreases with increasing velocity." This fact is the main motivation for the proposed mechanism of tube instability.

In the process of studying the proposed mechanism we have performed a simple experiment blowing air on a cantilever circular cylinder lightly damped. Although this experiment showed a dramatic instability at Re = 1000, application of a stability criterion developed in the present work indicated the motion should be stable. This led to a second instability mechanism caused by a velocity gradient in the flow which was later found to exist. Reference [9] is another example of this new mechanism that seems to be the cause of vibration of bundled electrical conductors. This mechanism is very important for low-frequency structures lightly damped.

2. Stability Criteria for Drag Coefficient Decrease Case

If we consider a circular cylinder vibrating in line with a steady flow near the critical Reynolds number the drag coefficient will decrease sharply when the motion is counter to the flow. This occurs because the relative velocity, and corresponding Reynolds number, will increase. The reverse is also true, i.e., for motion in the direction of the flow the drag coefficient will increase. Depending on the slope of the drag coefficient versus Reynolds number curve the net energy input to the vibrating cylinder, caused by the drag force, is positive. Thus, self-induced vibrations can be sustained at an amplitude such that this net energy is dissipated by damping.

2.1 Drag Coefficient versus Reynolds Number

Consider Fig. 1. The sharp drop in the drag coefficient at Reynolds number approximately 3×10^5 occurs because the flow in the boundary layer becomes turbulent before separation, moving the separation point farther downstream and thereby reducing the form drag. Since at high Reynolds numbers the total drag is very near the form drag, the drag force decreases [8] when the flow is increased past the critical Reynolds number. We proceed to determine the conditions under which self-induced vibrations of circular cylinders in a high steady flow can occur.

The basic assumption in this work is that the static drag coefficient versus Reynolds curve applies in the dynamic situations, i.e., the time between separation and reattachment of the boundary layer must be small compared with the natural period of the cylinder. Schlichting [10], page 381, shows that the transition from laminar to turbulent flow, in a laminar boundary layer with an artificial disturbance, occurs during a time $t \ll 1/60$ sec. This suggests that for low-frequency cylinders, say < 50 Hz, our basic assumption in using the static curve is justified.

2.2 Flow Across Rigid Cylinders

The equation of motion for a rigid cylinder, spring supported, lightly damped, is

$$M\ddot{x}(t) + C\dot{x}(t) + Kx(t) = \frac{1}{2}\rho_\ell c_D (U_o - \dot{x})^2 DL \tag{1}$$

where M, D, L are the cylinder mass, diameter and length, respectively. C and K are the damping and stiffness coefficients. U_o is the steady flow velocity. ρ_ℓ is the liquid density and c_D is the drag coefficient.

For small oscillations about the static equilibrium position, the c_D versus Re curve can be approximated in the neighborhood of (Re_o, c_{D_o}) by

$$c_D = c_{D_o} - b(Re - Re_o) \tag{2}$$

where

$$c_{D_o} = c_D(Re_o) = c_D\left(\frac{U_o D}{\nu}\right) \tag{3}$$

ν is the fluid kinematic viscosity, and $b>0$ for $2 \times 10^5 < Re < 5 \times 10^5$ approximately. Equation (1) can be written

$$\ddot{x}(t) + 2\xi\omega\dot{x}(t) + \omega^2 x(t) = \left[c_{D_o} + \frac{bD}{\nu}\dot{x}(t)\right] a\left[U_o - \dot{x}(t)\right]^2 \tag{4}$$

where

ξ - critical damping fraction

ω - angular natural frequency

$a = \frac{\rho_\ell DL}{2M}$, constant

We obtain the static deflection x_{st}, by setting $x(t) = \dot{x}(t) = 0$ in eq. (4)

$$x_{st} = \frac{c_{D_o} a U_o^2}{\omega^2} \tag{5}$$

For stability of the system, consider small oscillations about the static equilibrium position, i.e., let

$$x(t) = \delta x(t) \cos \omega t + x_{st} \tag{6}$$

We want to investigate the conditions for stability, i.e., under what conditions the vibration amplitude $\delta x(t)$ increases with time.

Substituting eq. (6) into (4) and equating the terms in sin ωt and cos ωt we obtain

$$\delta\ddot{x}(t) = \left[\frac{abDU_o^2}{2\nu} - a\, c_{D_o} U_o - \xi\omega\right] 2\delta\dot{x}(t) \tag{7}$$

$$\delta\dot{x}(t) = \left[\frac{abDU_o^2}{2\nu} - a\, c_{D_o} U_o - \xi\omega\right] \delta x(t) \tag{8}$$

thus, the condition for stability is

$$\frac{abDU_o^2}{2\nu} = a\, c_{D_o} U_o - \delta\omega < 0 \tag{9}$$

or

$$\boxed{b < \frac{2\nu}{DU_o^2}\left(c_{D_o} U_o + \frac{\xi\omega}{a}\right) = b_c} \tag{10}$$

where b_c is the critical value of b. Note that for very lightly damped systems, i.e., $\xi \sim 0$, the condition for stability reduces to:

$$b < \frac{2}{DU_o}\; c_D = \frac{2c_{D_o}}{Re_o} = b_c \tag{11}$$

Suppose we can represent the curve c_D vs Re by

$$c_n = m\, Re^n \tag{12}$$

which is linear in a log-log graph.

By definition

$$b = -\left(\frac{dc_D}{dRe}\right)_{Re_o} = -\, m\, n\, Re_o^{\,n-1} \tag{13}$$

Using eq. (11), (12) and (13) for the critical value of $b = b_c$, we have

$$b_c = \frac{2c_{D_o}}{Re_o} = \frac{2m\, Re_o^{\,n}}{Re_o} = -\, m\, n\, Re_o^{\,n-1} \tag{14}$$

or $n = -2$

this means that for $n \leq -2$, $b \geq b_c = \frac{2c_{D_o}}{Re_o}$, i.e., instability occurs. Thus, in Fig. 1 the region of instability corresponds to those portions of the curve log c_D vs log Re that have a slope ≤ -2, as shown in Fig. 1.

We should recall that the above conclusion refers to the special case $\xi \simeq 0$. When this is not the case, eq. (10) gives the full stability criterion. It is seen that the higher the damping the more stable the system will be, as expected. Also, the higher $\omega M = \sqrt{KM}$ the more stable the system will be (increasing the stiffness or mass will tend to stabilize the structure).

Again, referring to the special case $\xi \simeq 0$, we note the instability condition $n \leq -2$ for the slope of the curve c_D vs Re in log-log scale was expected since the drag force increases with the square of the relative velocity.

2.3 Flow Across Simply-supported Flexible Cylinders

The actual conditions of the steam generator U-tubes can be better represented by simply-supported single or multi-span circular beams. We now consider the stability criterion for the system of Fig. 2. The equation of motion is

$$EI\,\frac{\partial^4 v}{\partial x^4}(x,t) + c\,\dot{v}(x,t) + m\,\ddot{v}(x,t) = \frac{1}{2}\,\rho_\ell\left[U_o - \dot{v}(x,t)\right]^2\left[c_{D_o} + \frac{bD}{\nu}\,\dot{v}(x,t)\right] D \tag{15}$$

where all the symbols have the same meaning as in the previous section. Let us use Ritz method to approximate the displacement field

$$v(x,t) = A(t) f_1(x) \tag{16}$$

where

$$f_1(x) = \sin\frac{\pi x}{\ell} \tag{17}$$

is the fundamental mode shape of a hinged-hinged beam. Substituting eq. (16) and (17) with (15) and integrating along the span, we obtain

$$\ddot{A}(t) + 2\xi\omega\dot{A}(t) + \omega^2 A(t) = a''\left\{c_{D_o}\left[U_o^2 - \frac{4U_o}{\pi}\dot{A}(t) + \frac{1}{2}\dot{A}(t)^2\right]\right.$$

$$\left. + \frac{bD}{\nu}\dot{A}(t)\left[\frac{2}{\pi}U_o^2 - U_o\dot{A}(t) + \frac{4}{3}\dot{A}(t)^2\right]\right\} \tag{18}$$

where $a'' = \dfrac{\pi\rho_\ell D}{4m}$ (19)

Again considering small perturbations about the static equilibrium position, we let

$$A(t) = \delta A(t)\cos\omega t + A_s t \tag{20}$$

where

$$A_s t = \frac{a'' c_{D_o} U_o^2}{\omega^2} \tag{21}$$

Following the same procedure as in the previous section we obtain the stability criterion for simply-supported flexible cylinders

$$\boxed{b < \frac{2\nu}{DU_o^2}\left(c_{D_o} U_o + \frac{\pi\xi\omega}{2A''}\right) = b_c} \tag{22}$$

3. Stability Criterion for Velocity Gradient Case

Now we will consider a different mechanism for flow-induced vibrations. This mechanism was motivated by an experiment done by one author [3] to investigate the mechanism discussed in §2. We have noticed a very strong instability at Reynolds numbers approximately 1,000, i.e., much lower than the critical value, thus eliminating the occurrence of that type of instability.

3.1 Spatial Variation of Velocity

In order to explain this new type of instability, we noticed that the flow was not uniform, i.e., there was a velocity gradient which was responsible for a net energy input to the vibrating cylinder, as will be shown next.

We will now consider 3-dimensional vibrations of a cantilever flexible cylinder with a non-uniform flow near the free end, as shown in Fig. 3.

3.2 Gradient Flow Across a Cantilever Flexible Cylinder

The equation of motion in the y-direction is:

$$EI\frac{\partial^4 v}{\partial x^4} + c\,\dot{v} + m\,\ddot{v} = f_{Dy}(x,t)\;[u_1(x - (\ell - D_T)] \tag{23}$$

where $f_{Dy}(x,t)$ is the drag force per unit length along the cylinder and where $u_1(x-x_o)$ is the unit step function and the remaining symbols as previously defined. A similar equation applies in z-direction. Now let

$$v(x,t) = \frac{1}{2}A(t)\,f_1(x) \tag{24}$$

$$w(x,t) = \frac{1}{2}B(t)\,f_1(x) \tag{25}$$

where $f_1(x)$ is the cantilever beam fundamental mode shape given in reference [11]. Thus, A(t) and B(t) are the tip deflections along the y and z axes, respectively. The drag force per unit length along the cylinder is given by the vector

$$\underline{F}_D(x,t) = (f_{Dy}(x,t),\, f_{Dz}(x,t)) = \frac{1}{2}\rho_\ell D c_D|\underline{U}-\underline{v}|\,(\underline{U}-\underline{v}) \tag{26}$$

where $\underline{v}$ is the velocity vector of a generic point x of the cylinder.

Again, substituting eq. (24) into (23) and integrating along the span we obtain

$$\ddot{A}(t) + 2\xi\omega\dot{A}(t) + \omega^2 A(t) = C'\;|\underline{U}-\underline{v}|\;(\underline{U}-\underline{v})_y \tag{27}$$

where ξ and ω are the critical damping fraction and angular natural frequency, respectively.

C' is given by

$$C' = \frac{\rho_\ell D\ C_D\ D_T}{.7829917558\ m\ \ell} \tag{28}$$

and a similar equation is obtained for the z-direction, following a procedure [3] similar to that in §2 in which we considered small perturbations about the static equilibrium position. For α, as shown in Fig. 4, near $\pi/2$, i.e., $\alpha = \pi/2 - \varepsilon$, where ε is small, we obtain the conditions for instability.

$$e\left[1 - \frac{C'U_o}{\omega}\frac{\varepsilon^3}{2}\frac{\delta A}{\delta B}\right] > \omega\frac{\delta A}{\delta B}\left[1 + \frac{\xi\omega}{C'U_o}\right] - \frac{\omega\varepsilon}{2}\left[\xi + \frac{C'U_o}{2\omega}\right] \tag{29}$$

and

$$e\left[1 + \frac{2\omega\varepsilon}{C'U_o}\frac{\delta A}{\delta B}\right] > \omega\frac{\delta A}{\delta B}\left[1 + \frac{\omega\xi}{C'U_o}\right] + \frac{\omega^2}{C'U_o\varepsilon}\left[1 + \frac{2\xi\omega}{C'U_o}\right] \tag{30}$$

we can see that in the limit as $\varepsilon \to 0$ we have

$$e > \omega\frac{\delta A}{\delta B}\left[1 + \frac{\xi\omega}{C'U_o}\right] \tag{31}$$

and

$$e > \infty \tag{32}$$

Obviously, eq. (32) cannot be satisfied meaning that the motion is always stable for $\alpha = \pi/2$. However, for ε small but different from zero eq. (29) and (30) will give the conditions for instability.

As an example, consider

$\alpha = 85^o$ or $\varepsilon = 5^o = .08727$ rad

$\frac{\delta A}{\delta B} = 5$ and $\xi = .005$

Eq. (29) and (30) give the results shown in Table I. It can be seen that eq. (30) is the limiting condition for instability.

It is clear that the ellipsis axes must not coincide with the direction of flow, i.e., for instability the angle α must be slightly different from $\pi/2$. This was observed in the experiment performed by the author and also in the experiment described in Reference [9]

4. Non-linear Numerical Solution for Combined Case

We now proceed to the solution of the non-linear equations of motion of circular cylinders vibrating in a steady non-uniform flow allowing for variations in the drag coefficient c_D with Reynolds number. Thus, we will be able to analyse both problems described in §2 and §3.

4.1 Equations of Motion

Consider Fig. 5. For generality we will allow different boundary conditions in plane xy and xz such that the fundamental frequencies in these planes can be different. The equation of motion in the y-direction is

$$EI\frac{\partial^4 v}{\partial x^4} + c_y\ \dot{v} + m\ \ddot{v} = f_{Dy}\ (x,t)\ [u_1(x-a^*)-u_1(x-b^*)] \tag{33}$$

where the symbols have the same meaning as before. The drag force per unit length $f_{Dy}(x,t)$ is given by eq. (26), where c_D is now a function of Re and similar equations apply in the z-direction. We need to define the dependence of the drag coefficient c_D on the Reynolds number. From Reference [12] it is seen that a good representation for the drag coefficient behavior is that c_D is constant for Re $\leqslant (Re)_1$; is constant at a lower value for Re $\geqslant (Re)_2$;

and varies linearly as a function of log Re between. The break-points in this representation are functions of geometry [12].

4.2 Numerical Solution

An efficient numerical scheme was developed to integrate eq. (35), as described in Reference [3]. A computer code based on this scheme was used to obtain the results of §5.

The computer code has the capability of dealing with several cases of vibrations induced by flow. The two basic vibration mechanisms are the negative slope in the c_D vs Re curve described in §2 and a flow with a velocity gradient described in §3.

5. Results and Comparison with Experiments

5.1 Stability Criteria

The stability criteria developed in §2 and §3 have been verified by the computer code and for all cases considered those criteria were in agreement with the code [3].

5.2 Comparison with a Tube Bundle Experiment

Reference [13] deals with flow-induced vibrations of tube banks. For in-line tube banks with pitch diameter ratio 1.34 a very large increase in the longitudinal vibration amplitude occurs at a flow velocity of .643 m/s. At this velocity the amplitude is

$$\frac{A}{D} \times 10^3 \simeq 45 \qquad (34)$$

Reference [12] gives several curves c_D vs Re for a single cylinder of diameter D confined between parallel planes a distance h apart, in terms of the confinement ratio D/h. For a tube row with pitch-diameter ratio 1.34, the confinement ratio D/h = .75 gives the same average gap velocity in the experiments of References [12] and [13]. Extrapolating the results obtained with D/h given by Reference [12] to D/h = .75 we obtain the critical velocity of .63 m/s as shown in Fig. 6. This is in very good agreement with the experimental value of .643 m/s.

5.3 Discussion of Ringhals Steam Generator

Based on Reference [1], we have a sketch of the fretting defects as shown in Fig. 7. Although we do not have any numerical values to compare our calculations with, we have performed a computation trying to explain qualitatively the fretting scars shown in Fig. 7. This was achieved by considering different boundary conditions on planes xy and xz of Fig. 5, i.e., on the xy-plane we had clamped-clamped boundary conditions while on the xz-plane we considered simply-supported boundary conditions. Also, the direction of the flow was taken with the angle $\alpha = 45^o$ (see Fig. 5). The natural frequencies were 29.947 and 13.1947 in planes xy and xz, respectively. The trajectory of the midspan of the tube in the beginning of the motion is shown in Fig. 8. It was found that the amplitudes in both directions y and z increase with time, showing that the mechanism may be responsible for fretting scars as shown in Fig. 7. After 2.1 seconds from the start of motion there was a .7% increase in the initial value of z and a 2.5% increase in the initial value of y, showing the motion is unstable. Thus, scars in practically any orientation can occur, depending on the relative position between tube and baffle plate, i.e., the gap.

The most important result is that by assuming different frequencies in planes xy and xz, which can occur in practice, we have been able to show a net positive energy input to the tube that must be dissipated by fretting against the baffle plates.

5.4 Numerical Results for a Cantilever Cylinder Vibrating in a Velocity Gradient -

Comparison with an Experiment Performed at MIT

One author has performed an experiment at MIT blowing air over a flexible tube. The geometry is exactly the same as shown in Fig. 3. The experimental results are shown in Table II.

The velocity gradient causing the vibration was produced by the walls of the tube blowing the air and its value is not known. Also, as predicted in §3.1, we needed a small deviation of the angle α from 90^o in order to produce tube vibration. In our computer program we have used the following values of damping, velocity gradient and α to obtain

ξ = .0005

e = 60,000 m/s.m

α = 89^o

A_y = 20.8 mm

A_z = .335 mm

for the amplitudes along y and z axes, respectively. Thus, we see a very good agreement with the experimental values of Table II. We found the numerical results to be very sensitive to the value of α, e.g., by letting $\alpha = 88^o$ we must increase e = 90,000 m/s.m to obtain an amplitude of approximately 19 mm. This high sensitivity to α was also found during the experiment.

In all calculations the initial conditions were small perturbations from the static equilibrium position.

6. Conclusions

We have proposed two flow-induced vibration mechanisms of circular cylinders. Stability criteria for several cases were developed by linearization of the equations of motion and compared with the numerical solution of the non-linear equations. An efficient numerical method was adopted to solve the non-linear equations. We found that:

1) For both mechanisms all the stability criteria were validated by the computer code (§5.1).

2) For the negative slope in the c_D vs Re curve mechanism, eq. (10) and (22) give a quantitative way to increase stability, e.g., by increasing the natural frequency, increasing damping, decreasing the flow velocity, etc.

3) Good numerical agreement was found between a tube bundle experiment [13] and our calculations for in-line vibration of heat-exchanger tube banks as described in §5.2.

4) §5.3 suggests the proposed mechanism to be responsible for the unexpected instability found at the Ringhals 3 steam-generators. Reference [6] describing a similar experiment points out that the vibration amplitude decreased as flow increased which is in agreement with proposed mechanism since the c_D vs Re curve becomes flat again once the boundary layer flow is fully turbulent.

5) References [5], [8] point out that increasing the surface roughness of the cylinder (e.g., adding silk threads near the front stagnation line) lowers the critical Re region in model tests. This suggests the introduction of very superficial grooves in the tube surface to make the boundary layer flow turbulent at an earlier stage of SG operation.

6) Reference [9], Fig. 12, shows the motion buildup of a cylinder vibrating in a velocity gradient and it can be seen that it is very similar to the results obtained in this work. The small tilting of the ellipsis major axis with respect to the flow that was observed there was also calculated here.

References

[1] Communication between the Brazilian Nuclear Energy Commission and the Swedish Nuclear Authority, 1981.

[2] Communication between the Brazilian Nuclear Energy Commission and the Spanish Nuclear Authority, 1981.

[3] Ribeiro, S.G., "Mechanisms of Flow-induced Vibrations of Circular Cylinders in Crossflow," S.M. Thesis, MIT, January 1983.

[4] Blevins, R.D., "Flow-induced Vibration," Van Nostrand Reinhold Company, New York (1977).

[5] Humphreys, J.S., "On a Circular Cylinder in a Steady Wind at Transition Reynolds Numbers," J. Fluid Mechanics, vol. 9, pt. 4, December 1960, pp. 603-612.

[6] Lubin, B.T., Guerrero, H.N. and Kantayya, R.C., "Response of a Tube Bank to Crossflow-induced Excitation at Trans- and Supercritical Reynolds Numbers," Practical Experiences with Flow-induced Vibrations, Karlsruhe, Germany, 1979.

[7] Guerrero, H.N., Haslinger, K.H., Lubin, B.T., and Rossano, F.V., "Flow-induced Vibrations of a PWR Upper Guide Structure Tube Bank Model," Topical Meeting on Nuclear Reactor Thermal-hydraulics, October 1980, Saratoga, New York.

[8] Tietjens, O.G. and Prandtl, L., "Applied Hydro- and Aeromechanics," McGraw-Hill Book Company, Inc., New York, 1934.

[9] Cooper, K.R. and Watts, J.A., "Wind Tunnel and Analytical Investigations into the Aeroelastic Behaviour of Bundled Conductors," IEEE Transactions on Power Apparatus and Systems, vol. PAS-94, no. 2, March/April 1975.

[10] Schlichting, H., "Boundary Layer Theory," McGraw-Hill Book Company, Inc., New York, 1960.

[11] Blevins, R.D., "Formulas for Natural Frequency and Mode Shape," Van Nostrand Reinhold Company, New York, 1979.

[12] Richter, A. and Nandascher, E., "Fluctuating Forces on a Rigid Circular Cylinder in Confined Flow," J. Fluid Mechanics, vol. 78, pt. 3, 1976, pp. 561-576.

[13] Zukauskas, A and Katinas, V., "Flow-induced Vibration in Heat-Exchanger Tube Banks," Practical Experiences with Flow-induced Vibrations, Karlsruhe, Germany, 1979.

Table I Instability Conditions

$\frac{\omega}{C'U_o}$	Upper Limits on e/ω for Stability	
	Eq. (29)	Eq. (30)
1	5.01	8.86
5	5.12	12.17
10	5.25	13.50
50	6.25	19.39
100	7.50	26.04
200	10.00	39.22
500	17.50	78.64
1000	30.00	144.30

Table II Experimental Results for Cylinder Vibrating in Velocity Gradient [3]

U_o(m/s)	Vibration Amplitude of Free End along y-axis (mm)
1) 16.8	27
2) 16.5	19
3) 16.5	22
4) 16.0	18

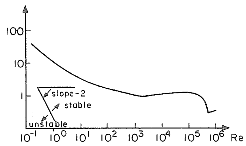

Figure 1 c_D versus Re Curve (from Reference [14])

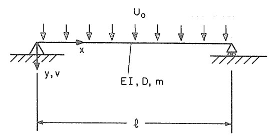

Figure 2 Simply-supported Flexible Cylinder under Uniform Flow

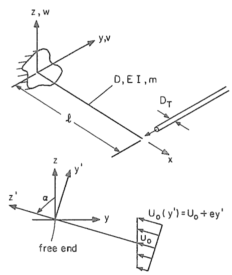

Figure 3 3-D Cantilever Cylinder Subject to a Velocity Gradient at the Free End

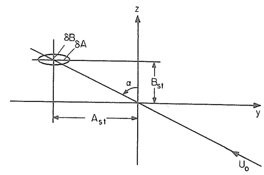

Figure 4 Small Elliptical Motion about the Static Equilibrium Position

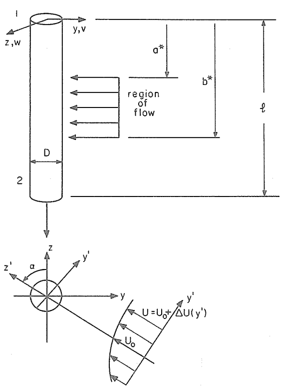

Figure 5 Geometry Considered in the Computer Code

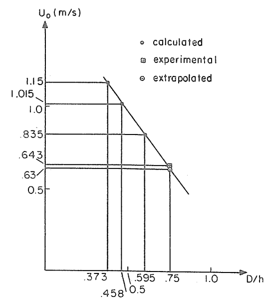

Figure 6 Extrapolation of Calculated Results to Determine Critical Flow Velocity

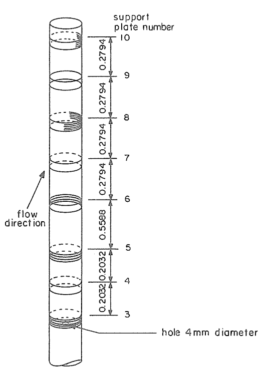

Figure 7 Fretting Scars on SG-tubes (dimensions in meters)

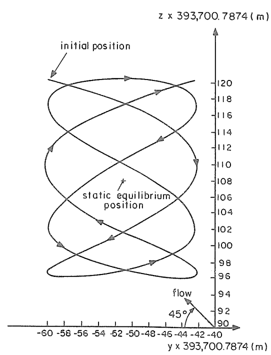

Figure 8 Tube Mid-span Trajectory in the Beginning of Motion